

CONFERENCES AND SYMPOSIA

PACS numbers: **42.79. – e**, **78.55. – m**, 78.67.Hc

Multifunctional far-field luminescence nanoscope for studying single molecules and quantum dots
(50th anniversary of the Institute of Spectroscopy, Russian Academy of Sciences)

I Yu Eremchev, M Yu Eremchev, A V Naumov

DOI: https://doi.org/10.3367/UFNe.2018.06.038461

Contents

Abstract. Far-field fluorescence spectromicroscopy of single quantum emitters (SQEs) (single molecules, quantum dots, color centers in crystals) is an actively developing field of modern photonics, which is in widespread demand in various applications in physics, chemistry, material sciences, life sciences, and quantum technologies. In this paper, we present a description of a multifunctional experimental setup which was developed in recent years at the Institute for Spectroscopy of the Russian Academy of Sciences. It allows measuring optical spectra and fluorescence images of SQEs, as well as their temporal behavior and luminescence kinetics, in a broad range of temperatures (from cryogenic to ambient). It is shown that the spatial coordinates of SQEs can be reconstructed with subdiffractional accuracy (up to a few angstroms). Some examples of the developed methods for multiparameter superresolution microscopy (nanoscopy) of materials and nanostructures are presented.

I Yu Eremchev [1,2], **M Yu Eremchev** [1,2,3], **A V Naumov** [1,2,4]
[1] Institute of Spectroscopy, Russian Academy of Sciences, ul. Fizicheskaya 5, 108840 Troitsk, Moscow, Russian Federation
[2] Moscow Institute of Physics and Technology (State University), Institutskii per. 9, 141700 Dolgoprudnyi, Moscow region, Russian Federation
[3] École Polytechnique Fédérale de Lausanne, Lausanne, Switzerland
[4] Moscow State Pedagogical University, ul. Malaya Pirogovskaya 1, 119882 Moscow, Russian Federation
E-mail: naumov@isan.troitsk.ru

Received 5 October 2018
Uspekhi Fizicheskikh Nauk **189** (3) 312 – 322 (2019)
DOI: https://doi.org/10.3367/UFNr.2018.06.038461
Translated by M L Skorikov

Keywords: luminescence, microscopy, nanoscopy, single molecule, quantum dot, color center, antibunching, kinetics, polymers, glasses, crystals, nanodiagnostics, cryogenic temperatures, Shpol'skii matrix, sensor, CdSe, NV-center

1. Introduction

Modern science and technology imposes a number of fundamental requirements on instruments used to investigate the properties of materials. In particular, solid state physics, physical chemistry, materials science, electronics, nanotechnologies, quantum technologies, and life sciences need nondestructive experimental techniques that combine ultrahigh sensitivity and high spatial and temporal resolution. Recent years have seen rapid advances in the field of optical nanoscopy, i.e., fluorescence microscopy with ultrahigh spatial resolution, rewarded in 2014 with the Nobel Prize in Chemistry [1–3]. Many of these methods are based on the detection of fluorescence images of single quantum emitters (SQEs) (such as organic dye molecules, nanocrystals, and nanoparticles) embedded in investigated objects to serve as nanoprobes. This approach relies on the fact that computer analysis of the image of an isolated (single) quantum emitter with dimensions that are much smaller than the wavelength of emitted light makes it possible to reconstruct the spatial coordinates with a much better accuracy than the Abbe diffraction limit ($\lambda/2\mathrm{NA}$), where NA is the aperture.

By separately detecting and reconstructing the coordinates of a large number of probe SQEs, it is possible to reproduce the structure of an object tagged with such nanoprobes with subdiffraction accuracy, i.e., to obtain a nanoscopic image. Approaches exist that enable the reconstruction of all three spatial coordinates of an SQE, i.e., offer

three-dimensional nanoscopy of materials and structures [4, 5]. Thus, three-dimensional nanoscopy can be implemented using elements of adaptive optics to instrumentally modify the point-spread function (PSF) of SQEs [6]. Finally, a rapidly developing area in the field of nanodiagnostics of condensed media, materials, and devices is the use of combination techniques exploiting simultaneously the potential of spectroscopy, optical microscopy, and other diagnostic methods like atomic-force microscopy (AFM) and electron microscopy.

The capabilities of these methods are considerably enhanced in the case of 'multicolor' fluorescence nanoscopy, where the images from individual emitters are recorded at different wavelengths [7]. This idea can be implemented most productively at cryogenic temperatures, because the widths of zero-phonon lines (ZPLs) of individual impurity molecules observed at low temperatures are several orders of magnitude smaller than the shifts of ZPL frequencies induced by local inhomogeneities in the structure of the investigated material. Therefore, 'multicolor' nanoscopy can be implemented by the serial–parallel excitation of ZPLs of single probe molecules by a frequency-tunable narrowband laser [8]. Furthermore, the fact that ZPLs are extremely sensitive to the parameters of local environment of a given molecule offers the potential of nanodiagnostics of the structure and local dynamics of the material.

On the other hand, measurements of the spectra of SQEs and investigations of their temporal dynamics and their dependences on various external factors (electric and magnetic fields, temperature, hydrostatic pressure) offer a unique possibility for fundamental studies of intra- and intermolecular interactions at the level of an individual emitter and its closest environment. Particular interest in this research field is stimulated by studies of emitting nanoobjects with complex internal structure like macromolecular complexes [9], semiconductor nanocrystals (quantum dots) [10–13], nanodiamonds with color centers [14], and light-emitting biological objects [15, 16]. The field of fluorescence nanoscopy also attracts much attention in view of the very high potential of these techniques in biodiagnostics [17]; in studies of metamaterials, nanoantennas, plasmonic structures, and microcavities [18–20]; and in devices for modern (in particular, organic) optoelectronics and photovoltaics [21, 22]. Nanoscopy techniques make it possible to reveal in direct experiments the fundamental relations between microscopic characteristics of nanostructured (meta)materials with their effective macroscopic parameters [23]. Moreover, dynamic processes can be investigated with modern experimental equipment on extremely short timescales down to femtoseconds [24].

Joint implementation of the entire set of the discussed experimental techniques opens up unprecedented opportunities both for performing a broad range of fundamental tasks in numerous fields of modern science and technology and for applications in technological processes like the synthesis of materials with predesigned properties and modern ultrapure materials; environmental monitoring; and the development of the instrument base of physical chemistry, biophysics, and nanotechnologies.

Our research group from the Laboratory of Electronic Spectra of Molecules at the Institute of Spectroscopy, Russian Academy of Sciences, working in collaboration with the University of Bayreuth (Germany), was one of the first teams in Russia to begin experimental work on single-molecule spectroscopy and microscopy aimed at the investigation of the low-temperature dynamics of disordered solids. To date, this team has obtained a number of novel results in this field, which gained international recognition (see [25–36], as well as reviews [8, 37] and references therein). In this publication, we describe the unique hardware and software facility designed at the Laboratory of Electronic Spectra of Molecules and the methods and approaches in the field of fluorescence spectromicroscopy of SQEs developed by our team. We demonstrate how the developed methods can be used in studies of the spectra of single organic molecules and semiconductor colloidal quantum dots.

2. Spectromicroscopy of single pointlike (quantum) emitters

The spectromicroscopy of single molecules is a relatively new direction in optical spectroscopy. The absorption spectra and fluorescence excitation spectra of single molecules in an organic polycrystal were recorded for the first time on the cusp of the 1990s [38, 39]. In the thirty years since then, this field has been the subject of intense research and has become one of the hottest in physics, physical chemistry, biophysics, and related areas of science. This technique is so attractive owing to the possibility of investigating physical and chemical properties of matter at the level of individual molecules. In addition, the high sensitivity of the optical spectra of single impurity chromophore centers to the parameters of the closest (nanometer) environment allows using them as spectral nanoprobes. ZPLs of impurity centers, which, as a rule, are observed at cryogenic temperatures, are especially informative and most sensitive to the parameters of the closest environment. This circumstance offers a unique opportunity to study the local internal dynamics of condensed matter and provides a technique to characterize the material structure at the nanometer level.

Today, the spectromicroscopy of single molecules has become a powerful tool for the investigation of the low-temperature dynamics of disordered solids (see [8] and references therein). In particular, dynamic processes in the matrix manifest themselves in the individual spectra of single molecules as stepwise changes in the frequencies and widths of the spectral lines, and at the level of the entire ensemble of dopant molecules they lead to the broadening of the spectra (optical dephasing and spectral diffusion). Therefore, by observing the spectral dynamics of impurity chromophore molecules, we can obtain information on low-energy excitations in disordered media. Indeed, studies of the low-temperature dynamics of disordered solids at the microscopic level determined the initial development of single-molecule spectromicroscopy (Fig. 1).

One of the most promising directions of single-molecule spectromicroscopy is the development of fluorescence nanoscopy techniques, i.e., far-field diagnostics of solids based on the fluorescence images and spectra of single dopant molecules used as markers. It is well known that the spatial resolution of classical optical microscopes is limited to about half of the wavelength of light because of diffraction. Progress in high-resolution techniques based on single-molecule fluorescence microscopy helped overcome the classical diffraction limit in far-field optical microscopy. These techniques build upon the basic possibility of reconstructing the spatial coordinates of a pointlike emitter with

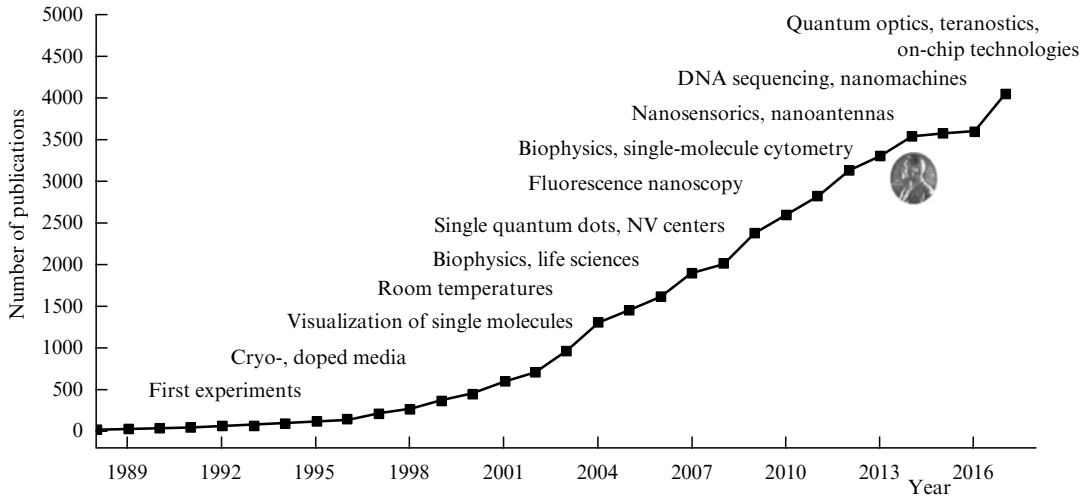

Figure 1. Number of publications with keywords 'single molecule' since 1988 according to the Web of Science international database (as of June 2018). The plot also shows the main application areas of the spectromicroscopy of single quantum emitters.

subdiffraction accuracy via computer analysis of its fluorescence image.

The first studies on the imaging of single molecules began in the early 1990s [40]. With the advent of high-sensitivity two-dimensional detectors based on charge-coupled devices (CCDs) and improvements in other optical components, it was demonstrated that the lateral coordinates can be determined with an accuracy as good as several nanometers [41]. After the detection of single-molecule luminescence became possible at room temperature, interest in these techniques on the part of researchers working in the life sciences increased explosively [42]. In particular, revolutionary optical technologies appeared in such areas as DNA sequencing [43], flow cytometry [44], and cell biology and teranostics [45].

By the second half of the 2000s, the intense development of fluorescence nanoscopy led to the creation of methods and commercially available instruments for the optical microscopy of biological objects with spatial superresolution: STochastic Optical Reconstruction Microscopy (STORM [46]), PhotoActivated Localization Microscopy (PALM [47]), etc. Since the diagnostics of extended objects typically require a large number of single molecules and their high spatial density, nanoscopy techniques employ various contrivances to attain the separate detection of molecules residing within the same diffraction-limited volume. Thus, supplementary laser sources used for molecule switching (photobleaching of individual molecules) can be introduced into the scheme or individual molecules can be discriminated according to additional attributes.

One of our approaches to the implementation of fluorescence nanoscopy is based on the observation of ZPLs and the effect of considerable inhomogeneous broadening of the dopant optical spectra in solids [28]. It is well known that the homogeneous width of ZPLs of single molecules in disordered organic solids at cryogenic temperatures is several orders of magnitude (up to $10^5 - 10^6$) smaller than the width of inhomogeneously broadened spectra. Thus, the positions (frequencies) of ZPLs for different molecules are distributed over a broad frequency range, which enables selective excitation of the luminescence of individual chromophores by tuning the laser frequency to resonance with the electronic transition frequencies in different molecules.

This approach makes it possible to simultaneously determine the spatial coordinates and individual fluorescence excitation spectra for huge ensembles of impurity molecules. In fact, the new technique allows us to detect all effectively emitting molecules within the microscope field of view while retaining the full set of data on the individual spectral parameters and coordinates of each molecule. These data can be subsequently processed offline, e.g., to reveal fundamental relations between the local characteristics of the investigated object and its structure, as well as the macroscopic characteristics of the material [29, 36]. In the framework of this approach, fluorescence nanoscopy can be used in a broad range of applications in materials science and nanotechnology.

Considerable progress in SQE spectromicroscopy has taken place with the appearance of new types of SQEs: semiconductor quantum dots, color centers in nanocrystals, dielectric and hybrid nanoparticles, and macromolecular complexes. For example, the optics of semiconductor quantum dots [48, 49] and spectroscopy of single color centers in nanodiamonds [50] have become separate fields of research in and of themselves. Recently, a growing number of studies have been devoted to the photonics of SQEs incorporated in artificial nanostructured (meta)materials and structures like molecular machines, hybrid particles, nanoantennas, and microcavities. This work finds applications in quantum optics, nanosensorics, micro- and nanoelectronics, and 'laboratory-on-chip' technologies (see, e.g., [51, 52]).

Hardware and software solutions for single-molecule spectromicroscopy techniques are also being constantly upgraded with the appearance of new photonic technologies and instruments: laser and spectral equipment, high-sensitivity detectors, optomechanics, multielement aspheric optical components, and adaptive optics. Impressive results have been obtained using combination techniques where the methods of fluorescence nanoscopy with SQE detection are used together with AFM [53, 54] or electron microscopy [55]. Finally, rapid progress is taking place in computer hardware, as well as in software solutions and algorithms, which represent an integral and essential part of nanoscopy techniques. This makes it possible to implement nanoscopy on the basis of conventional personal computers or even smartphones [56].

3. Multifunctional luminescence nanoscope

Figure 2 shows the basic layout of the multifunctional fluorescence nanoscope for the investigation of single molecules and quantum dots developed over recent years at the Laboratory of Electronic Spectra of Molecules at the Institute of Spectroscopy. In this and the following sections, we present the main units of this hardware and software facility, describe the measurement techniques, and discuss particular examples of how this facility is utilized for studies of the photophysical properties of SQEs of different natures and for multiparameter diagnostics of complex-structured condensed media and nanoobjects.

3.1 Excitation light sources

Sources of radiation ('Laser' block in Fig. 2) used for the excitation of photoluminescence with controlled characteristics are of fundamental importance for the techniques of spectromicroscopy of single molecules and their applications in nanoscopy. Part of the described measurement facility is a set of different laser systems, which are listed below.

(i) Solid-state lasers emitting cw radiation at a wavelength of 532 nm with a variable power of up to several watts.

(ii) Coherent CR-599 cw broadband (~ 8.3 GHz, or ~ 0.28 cm^{-1}) Rhodamine 6G laser with a linear cavity pumped by a Coherent Verdi V6 solid-state laser. Continuous tuning of the emission wavelength between 565 and 630 nm is performed using an intracavity birefringent filter that is computer controlled using an Arduino controller and specially written software. The emission power varies in the range of up to ~ 1 W.

(iii) Coherent CR-699 cw narrowband (~ 2 MHz, including fast fluctuations) Rhodamine 6G laser with a ring cavity pumped by a Coherent Verdi V6 solid-state laser and equipped with an Autoscan system for continuous tuning in a broad range of $\sim 565-600$ nm. Tuning and precise stabilization (to an accuracy of 2 MHz) of the emission frequency in this laser are performed using tunable Fabry–Perot etalons. The emission power is varied up to ~ 0.5 W.

(iv) Pico(femto)second laser system based on a Tema-150 femtosecond oscillator (Avesta Project Ltd.) with a pulse duration of 143 fs, a pulse repetition rate of 71.2 MHz, an emission wavelength of 1050 nm, and a power of 5.8 W. Using an OG2/1000-KTP electrooptical pulse picker (Avesta Project Ltd.), the pulse train can be 'thinned' to obtain a repetition rate from 1 MHz to single pulses. After frequency doubling (ASG-1050, Avesta), laser pulses at a wavelength of 525 nm were passed through a glass parallelepiped to become broadened to 2 ps owing to group velocity dispersion.

Radiation from a laser source can be modified or conditioned in some way according to the experimental requirements ('Radiation conditioning unit' block in Fig. 2). This can be done using radiation power stabilizers (based on a Pockels cell), pinhole spatial filters for the formation of Gaussian beams, components changing the state of polarization of light (half- and quarter-wave plates), or phase spatial light modulators (SLMs) for manipulating the parameters of the wave front of laser radiation. This block also incorporates devices for monitoring radiation wavelength (a light-absorbing gas cell filled with iodine vapor for the rough control of the laser wavelength with an accuracy of a few gigahertz, an echelle grating spectrometer, and a scanning confocal Fabry–Perot interferometer.

To provide the possibility of working in the wide-field epiluminescence microscope mode (with frontal illumination), this block features a long-focal-length epi-lens that ensures the uniform illumination of the microobjective lens field of view. Laser radiation is steered into one of the two microscopes (see Section 3.2) via a dichroic mirror (Semrock, Thorlabs) optimized for the spectral range of interest.

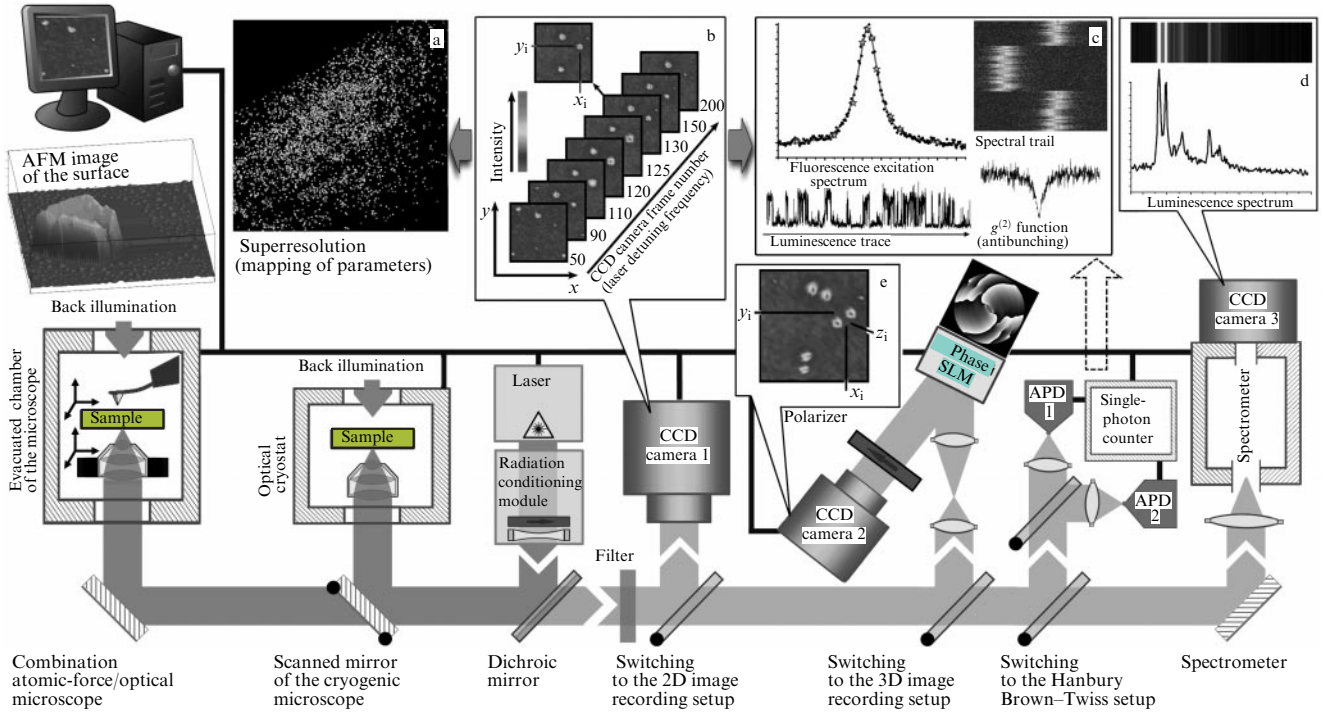

Figure 2. General layout of the multifunctional fluorescence nanoscope for studying single molecules and quantum dots. Different blocks and modules are described in the main text.

3.2 Optical cryomicroscope and combination scanning-probe/optical microscope

The measuring setup includes two separately installed microscopes.

1. Optical cryomicroscope based on an He^4 cryostat (RTI, Russia) and a Lakeshore-93 controller, which makes it possible to carry out experiments at temperatures from 1.5 K to room temperature. The temperature is measured by sensors attached in the immediate vicinity of the sample, which is mounted in a custom-designed sample holder with a translator module. The translator, capable of operating at cryogenic temperatures, together with the sample holder and a microobjective ($40\times$ magnification, NA $\sim 0.6-0.8$), is accommodated in the working chamber of the cryostat. The precise adjustment of the sample with respect to the microobjective in the axial direction (focusing) is carried out using a micrometer screw by flexing a specially shaped split metal part. The screw is rotated via a mechanical actuator placed outside. At temperatures $T > 4.2$ K, measurements are performed in He^4 vapor; in the temperature range between 2.17 and 4.2 K, above the surface of liquid He^4; and below 2.17 K, in superfluid He^4 under pumping.

2. The second part of the hardware setup consists of a custom-designed combination scanning-probe/optical microscope. The AFM (Nano Scan Technology) enables synchronous profiling of the sample surface with an accuracy of several nanometers, while the optical part allows measurements in the wide-field and/or confocal luminescence microscope mode.

The sample holder (Nano Scan Technology) provides controlled motion of the sample with an accuracy up to several angstroms along all three dimensions. The entire block is located in an airtight chamber, which makes it possible to carry out measurements in a vacuum or in a gas (e.g., noble-gas) atmosphere. The sample temperature can be varied in a range of up to several dozen degrees with respect to room temperature using a Peltier element or a 'cold finger' cooled by liquid nitrogen. The optical microscope is equipped in this case with dry and immersion high-aperture aberration-corrected objective lenses.

3.3 Detection units

Before the luminescence signal is received by a detection module, radiation comes through specially selected bandpass and longpass interference filters.

1. Measurements in the wide-field luminescence microscope mode (Fig. 2b) are carried out using Andor Luca or Andor Ixon Ultra high-sensitivity cooled electron multiplying CCD cameras (quantum efficiency exceeding 50% and 90%, respectively). The high sensitivity and quantum efficiency of these CCD cameras allow the detection of fluorescence images of individual SQEs using exposures starting as short as several milliseconds.

2. A separate module (Fig. 2e) is designated for measurements with instrumental engineering of the PSF (Point Spread Function used to precisely determine the depth at which SQEs are located with respect to the focal plane of the microobjective lens. For this purpose, this detection channel contains a phase SLM (based on a liquid-crystal matrix in our case) placed in the Fourier plane of the microscope to create a helical beam with the required properties. When a mask specially calculated taking into account the parameters of the microobjective and the optical setup is loaded into the modulator, the PSF can be modified in the desired way. In particular, the third (axial) coordinate can be reconstructed with the use of the double-helix PSF scheme, whereby, upon interaction with the phase mask, the image of each pointlike emitter is transformed into a two-lobe pattern oriented at an angle that is directly related to the depth of the emitter with respect to the focal plane of the microscope. These two-lobe images are recorded using high-sensitivity Andor Luca or Andor Ixon Ultra CCD cameras. This technique, proposed several years ago [57], has become increasingly widespread in three-dimensional nanoscopy systems [37, 54]. The calculation of a phase mask for this system is itself a difficult numerical problem of finding stable solutions to a wave equation in the form of superpositions of Laguerre–Gaussian modes with specified spatial characteristics [58, 59].

3. The next module (Fig. 2c) includes a scanning confocal microscope with signal detection in either a single-channel setup or in a conventional Hanbury Brown and Twiss (HBT) intensity interferometer with two detectors.

SQE fluorescence is detected by EG&G SPCM-200PQ avalanche photodiodes, possessing a quantum yield of $\sim 50\%$ at 600 nm and a dead time of 200 ns, operating in the single-photon counting mode. The detector time resolution is 1.3 ns; this is the width of the instrument response function determined by measuring the detector response to picosecond laser pulses (see Fig. 5 below). The photon and laser sync pulse arrival times are measured using a Becker&Hickl DPC-230 multichannel time-correlated single-photon counting unit with a time resolution of 165 ps.

In the HBT setup, the flux of photons from an SQE is divided into two channels by a 50% interference beamsplitter plate (Thorlabs) and recorded by two avalanche photodiodes. Much like in the preceding setup, the absolute times of photon arrival are measured in the two channels, after which the obtained sequences are used to determine the cross-correlation function.

4. The spectra of SQE luminescence are recorded using a homemade prism spectrometer with a spectral resolution of 0.5 nm (Fig. 2d) used with the microscope in the confocal mode; the signal is detected by an Andor Ixon Ultra CCD camera.

3.4 Methods of multiparameter fluorescence nanoscopy with the detection of single quantum emitters

The described setups were used for studies of photophysical characteristics of SQEs of various physical nature and chemical compositions, as well as for nanodiagnostics of complex solids and nanostructures. We used both known and originally developed techniques.

1. Detection of fluorescence images of SQEs in confocal scanning microscope and/or wide-field epiluminescence microscope modes. Figure 3 shows four consecutively taken frames of a CCD camera featuring room-temperature

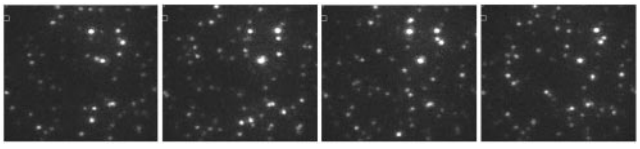

Figure 3. Consecutively recorded CCD camera frames with fluorescence images of single CdSeS/ZnS colloidal semiconductor quantum dots at room temperature. The accumulation time is 100 ms per frame. The frame size corresponds to a sample size of 20×20 μm.

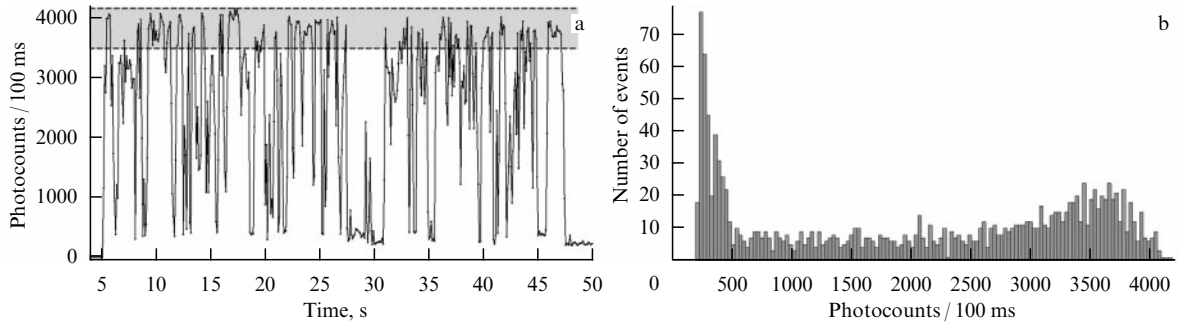

Figure 4. (a) Fluorescence trace recorded at room temperature for a CdSeS/ZnS colloidal semiconductor quantum dot. (b) The corresponding histogram of the fluorescence photon distribution. The accumulation time is 100 ms per point.

fluorescence images of single CdSeS/ZnS colloidal quantum dots deposited onto a glass substrate. Luminescence was excited by a cw single-frequency laser at a wavelength of 532 nm. The luminescence signal was accumulated for 100 ms per frame. The image size is 20×20 μm.

The intermittent character of luminescence from these quantum dots is clearly seen in Fig. 3. Processing the obtained images using specially developed identification and analysis software allows the reconstruction of the transverse (within the substrate plane) spatial coordinates of the quantum dots with nanometer accuracy.

Similar measurements can also be carried out at cryogenic temperatures (Figs 2a, b), and different experimental parameters (frequency, polarization, or power density of excitation radiation; sample temperature; etc.) can be varied.

2. Measurements of the parameters of ZPLs of a large number of single organic dye molecules embedded in solid-state matrices (low-molecular-weight organic glasses, polymers, polycrystals) within the microscope field of view in the temperature range from 1.6 to 70 K. For this purpose, the fluorescence images of all emitters found within the microscope field of view are recorded sequentially upon changing the frequency of a tunable narrowband laser (Fig. 2b). As a result, the images of individual molecules are identified and collated using originally developed software, which yields the fluorescence excitation spectrum for each molecule (upper left part of Fig. 2c).

These measurements (scanning of the laser frequency in the selected spectral range) can be done repeatedly, which makes it possible to determine the spectral trail of each molecule (upper right part of Fig. 2c), reflecting the spectral dynamics. In this way, notably, we investigated the processes of spectral diffusion and local structural relaxation in doped polymers and glasses [25, 30, 32]. Analysis of the temperature dependences of the single-molecule ZPL parameters in the temperature range up to several dozen kelvin makes it possible to study both tunneling and vibrational dynamics of the matrix, and, in particular, to investigate the microscopic nature of electron–phonon interaction and the phenomenon of the boson peak in disordered solids [26, 27]. In the most recent studies, we were able to record for the first time the spectrum of the quasi-localized low-frequency vibration mode in a polymer matrix (polyisobutylene) in the fluorescence excitation spectrum of single molecules of Mg-tetraazaporphyrin. It allowed the direct measurement of the energy and lifetime of single quasi-localized low-frequency modes. In addition, we observed spectral diffusion in an anomalously broad spectral range [60].

3. Measurement of fluorescence traces (time dependences of the fluorescence intensity) and photon distribution functions (photon statistics) for single molecules and quantum dots (lower left part of Fig. 2c). SQE fluorescence intensities at different moments of time can be measured in both the single-channel confocal microscope mode and the epiluminescence wide-field microscope mode with identification of fluorescence images of individual objects recorded by CCD detectors.

Figure 4a shows an example of a room-temperature fluorescence trace of a CdSeS/ZnS colloidal quantum dot (Sigma Aldrich) with the luminescence peak at 630 nm. We also show in Fig. 4b the histogram of luminescence photon distribution (photon statistics). The signal accumulation time at each point of the trace was 100 ms. The excitation laser power density was 60 W cm^{-2}.

The analysis of this kind of fluorescence traces and photon statistics carried out for single molecules of terrylene in a polymer matrix made it possible to identify relaxation processes in the medium with different rate (temporal) characteristics [31].

The microscopic nature of the luminescence blinking process in core/shell colloidal quantum dots was investigated by this method in [34, 35]. Theoretical analysis of the fluorescence traces and photon distribution functions measured for CdSe/ZnS quantum dots revealed two mechanisms of the transition between the radiative and nonradiative states of the quantum dots [34].

A study of the excitation power density dependence of the 'bright' and 'dark' state durations in CdSe/ZnS quantum dots demonstrated that transitions from the bright to dark state are related to internal Auger ionization, while the reverse transitions are of a tunneling character [35].

4. Zero-phonon fluorescence nanoscopy. This is a unique experimental method of serial–parallel multichannel detection of zero-phonon luminescence images of SQEs embedded in a solid using a cryogenic epiluminescence microscope/spectrometer [28, 37]. With this method, one can determine spatial coordinates with nanometer accuracy, detect individual ZPL spectra and fluorescence images of a huge number of single emitting impurities, observe changes in their spectra with time and temperature and with the application of external fields, and track the spatial shifts of single emitters. The analysis of spatiospectral correlations, as well as the search for fundamental relations between the ZPL characteristics of individual molecules (and their dependences on external parameters) and the molecule position in the matrix structure enables multiparameter nanodiagnostics of solids.

For example, the subsite structure of the primary spectral site in the absorption spectrum of terrylene dopant molecules in polycrystalline n-hexadecane was revealed in [29], and an original technique for local-field mapping in a solid film, which can be used as a method of microrefractometry, was suggested and implemented in [33, 36].

5. Finding all three spatial coordinates of single molecules and quantum dots with subdiffraction accuracy (from several to tens of nanometers) (Fig. 2e). This technique is based on the analysis of fluorescence images of SQEs, whose sizes are much smaller than the light wavelength, in an optical microscope. In the simplest case, the image of an SQE represents an Airy disk, whose central part can be well approximated by a two-dimensional Gaussian. The coordinates of the center of the image (coordinates within the image plane) can be obtained with an accuracy determined by the total number of detected fluorescence photons that form the image and the signal-to-noise ratio. The accuracy may be from just a few to hundreds of nanometers. As we described above, to determine the third, axial, coordinate of SQEs, the method of PSF engineering is used. A specially calculated diffractive optical element transforms the Airy function into a two-lobe function whose orientation angle depends on the distance between the point source being imaged and the microobjective focal plane. This makes it possible to determine the depth at which the point source is located within a thick sample. To calibrate this setup, i.e., to establish the relation between the SQE depth and the orientation angle of the two-lobe pattern, an SQE is shifted in the axial direction by a high-precision piezoscanner, whereby the coordinate can be controlled with nanometer accuracy. Using this setup, we were able for the first time to record ZPLs from single molecules of terrylene in frozen orthodichlorobenzene at a temperature of 4.5 K with the full reconstruction of their spatial location within the sample [37].

6. Measurement of SQE luminescence kinetics. To record the SQE luminescence kinetics, we use a setup based on pulsed picosecond excitation and time-correlated fluorescence-photon counting. In this experiment, the times of single-photon detection events with respect to the corresponding times of SQE excitation events are consecutively measured. The histogram of the distribution of these detection times has the form of an exponentially decaying function with a characteristic time determined by the fluorescence lifetime. Curve *1* in Fig. 5 shows a fluorescence kinetic curve of a single quantum dot (CdSe/ZnS, Sigma Aldrich) measured in this way in the confocal microscope setup. For comparison, curve *3* shows the response function of the detection system. The quantum dot was excited by ~ 2-ps-long pulses with a wavelength of 525 nm and a repetition rate of 1 MHz.

By approximating the luminescence decay curve with a monoexponential function, we can find the effective luminescence lifetime of a single quantum dot, which equals 13.5 ns in this case.

7. Measurement of the correlation function of luminescent SQEs.

Two different schemes can be used to record the second-order autocorrelation function $g^{(2)}(\tau)$. The first of them is suitable for measuring $g^{(2)}(\tau)$ in the range of delay times τ longer than the 'dead time' of the single-photon detection system (which is 200 ns in our case). In this scheme, we use the single-photon counting mode with the absolute arrival time of each photon being recorded. Then, the autocorrelation function can be calculated from the obtained sequence of photon arrival times.

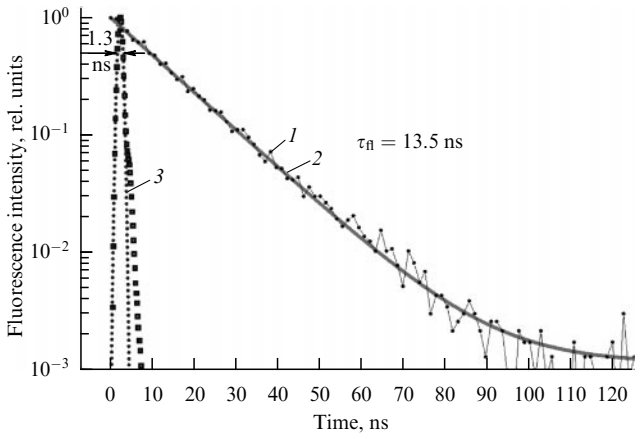

Figure 5. (Color online.) (*1*) Luminescence decay curve (kinetics) for a single CdSe/ZnS colloidal semiconductor quantum dot (black line) and (*2*) its approximation by a monoexponential dependence (red line). The independently measured response function of the detection system, which determines the time resolution in luminescence kinetics measurements, is shown for comparison by squares; curve *3* shows the result of its approximation by a Gaussian (blue dotted line).

In the second scheme, $g^{(2)}(\tau)$ can be measured over time intervals that are limited from below only by the time resolution of the detection system (about 1 ns in our setup). This is done using a conventional HBT intensity interferometer scheme (see Fig. 2). Similarly to the previous scheme, absolute times of photon arrival events are measured, but, in this case, these events are recorded in two detection channels rather than one. The obtained time sequences are then used to calculate the cross-correlation function:

$$g^{(2)}(\tau) = \frac{n_t}{N_{p1} N_{p2}} \sum N_1(t)\, N_2(t+\tau)\,; \qquad (1)$$

here, n_t is the number of time channels; N_{p1} and N_{p2} are the total number of photocounts detected in channels 1 and 2, respectively; and N_1 and N_2 are the signals in channels 1 and 2, respectively, at the corresponding moments of time.

Measurements of $g^{(2)}(\tau)$ in the (sub)nanosecond time range are interesting, because they allow the observation of photon antibunching for a nonclassical light emitter, e.g., a single molecule. Under continuous laser excitation, antibunching manifests itself as a characteristic dip in $g^{(2)}(\tau)$ around $\tau = 0$ ($g^{(2)}(0) \approx 0$), whose width is determined by the fluorescence lifetime (Fig. 6a) and whose depth is governed by the number of independently emitting objects and the ratio of their intensities. When an SQE is excited by pulses with a duration much shorter than the fluorescence lifetime, photon antibunching manifests itself in the 'vanishing' of the peak in $g^{(2)}(\tau)$ at zero delay (Fig. 6b).

In a real experiment, a small value of $g^{(2)}(0)$ is a good indicator of the fact that the object under study is a single-photon source; i.e., measurements of $g^{(2)}$ can be used to verify that the emitter is isolated from others and is indeed an SQE. It should also be noted that the rise of $g^{(2)}(\tau)$ near zero delay can be used to estimate the SQE fluorescence lifetime.

8. Finally, the capacity of the described hardware/software facility is considerably enhanced by the use of an AFM in combination with an ultrahigh-resolution epiluminescence microscope. Apart from performing the precise calibration of

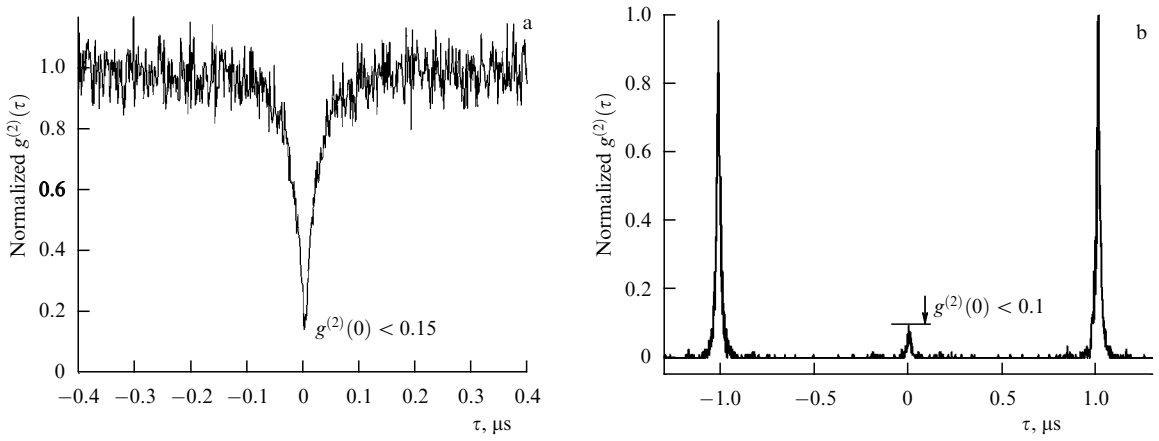

Figure 6. (a) Second-order luminescence autocorrelation function $g^{(2)}(\tau)$ for a single CdSeS/ZnS quantum dot measured at room temperature under excitation by a cw laser at a wavelength of 532 nm. (b) Function $g^{(2)}(\tau)$ for a CdSeS/ZnS quantum dot measured at room temperature under excitation by a pulsed laser with a pulse duration of 2 ps and a repetition rate of 1 MHz.

SQE spatial shifts and obtaining information on the absolute sizes of the structures with angstrom accuracy, there is a possibility to manipulate nanoobjects in the AFM contact mode and, of course, of surface profiling and characterization.

9. Algorithms and special software for computer control of the measurement routines and experimental data processing represent a distinct part of the described hardware/software facility. All blocks of the experimental setup have to be synchronized, with high-speed synchronization being required in certain cases (e.g., in correlation and kinetics measurements). Different modules serve as the main controller in the experimental setup, depending on the specific task: a Becker&Hickl DPC-230 time-correlated single-photon counting unit, an NST AFM controller, homemade controllers based on Arduino boards, or a Stanford SR400 control unit.

10. Software for image processing and specific statistical processing of large databases was developed in-house [8] and includes algorithms and modules for noise filtering; identification of individual images and their analysis, taking into account the PSF; consistent identification of images in repeated measurements, in particular, upon varying the experimental parameters (temperature, excitation laser power, and polarization); taking into account slow image drifts; etc. The developed software enabled realization of multiparameter (hyperspectral) nanoscopy of materials with complicated internal structures [8, 28, 36].

4. Accuracy of reconstruction of the coordinates of single quantum emitters

A basic question of the far-field localization microscopy (nanoscopy) concerns the accuracy of the reconstructed coordinates of single pointlike emitters, obtained by processing fluorescence images whose size is determined by diffraction in the optical elements of the microscope. In the first approximation, the accuracy $\sigma_{x,y}$ is determined by the width σ_{PSF} of the microscope PSF and the number N of photon counts that form the diffraction-limited image:

$$\sigma_{x,y} = \frac{\sigma_{\mathrm{PSF}}}{\sqrt{N}}\,. \qquad (2)$$

A more accurate formula takes into account the discreteness of the image (relation between the PSF width and the spatial discretization pitch) and the occurrence of parasitic noise [61]:

$$\sigma_{x,y} = \sqrt{\left(\frac{\sigma_{\mathrm{PSF}}^2 + a^2/12}{N}\right)\left(\frac{16}{9} + \frac{8\pi\sigma_{\mathrm{PSF}}^2 b^2}{a^2 N}\right)}\,, \qquad (3)$$

where a is the CCD camera pixel size and b is the level of noise (parasitic illumination).

To experimentally investigate the dependence of the accuracy of coordinate reconstruction on the number of photons, we can locate an SQE with a characteristic size much smaller than the wavelength within the microscope field of view and record luminescence images on a two-dimensional detector for different accumulation times or laser excitation intensities. It should be noted that, in the case of single quantum dots or single molecules, fluorescence may fluctuate over broad time and intensity ranges, even under continuous excitation at a fixed wavelength. Then, correct data analysis requires that the obtained coordinate sets be sorted according to the number of photocounts forming the images. As a result, for each of the required intervals of the image 'brightness' (horizontal gray band in Fig. 4a) we obtain a distribution of reconstructed coordinates, which can be used to estimate the accuracy under consideration. If the spatial drift of the image during the experiment can be disregarded or compensated, the obtained distribution of reconstructed coordinates will be close to a normal one, and its standard deviation will yield an estimate for the accuracy of coordinate reconstruction in a single measurement with a given number of photons.

Figure 7a shows an example of the distribution of reconstructed coordinates for an single emitting CdSe/ZnS quantum dot (with an emitting core size of 4.2 nm). The images were obtained using a Carl Zeiss 100× microobjective lens (NA = 1.3) and formed by ~ 3000 photocounts each. The standard deviation in this case is 3.5 nm (70% of coordinates reconstructed with subdiffraction accuracy fall within a 7-nm interval).

Figure 7b shows the dependence of the accuracy of x and y coordinate reconstruction (standard deviations of x (squares) and y (circles) coordinate distributions) on the number of

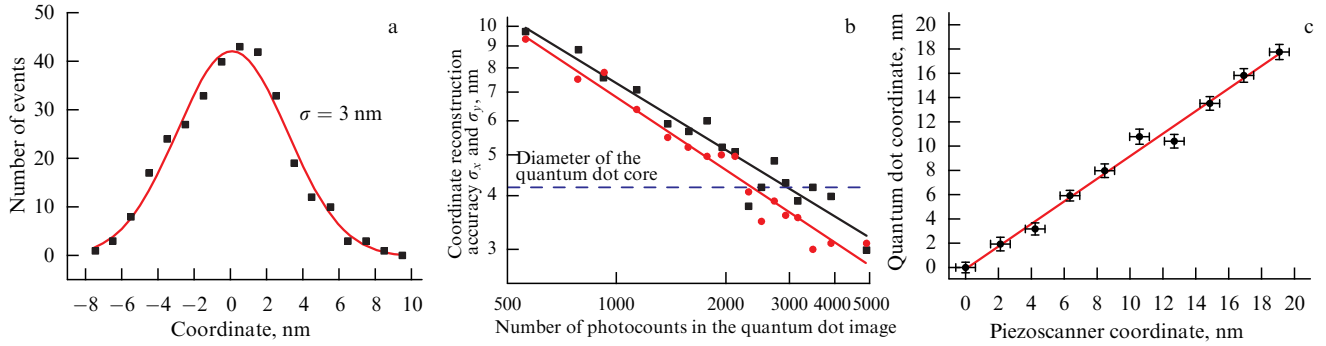

Figure 7. (a) Example of a distribution of reconstructed coordinates for a single CdSe/ZnS quantum dot (the emissive core size is 4.2 nm); luminescent images were obtained using a Carl Zeiss ×100 microobjective lens (NA = 1.3) and formed by ~ 3000 photocounts each. (b) Accuracies of x (squares) and y (circles) coordinate reconstruction versus the number of photocounts. (c) Dependence of the reconstructed value of the x coordinate of a single quantum dot on the actual spatial shift of the sample.

photocounts for the same quantum dot. The dependences behave like a power law with an exponent close to −0.5. It is noteworthy that this behavior persists to accuracies comparable to or even better than the size of the quantum dot core, where photoinduced electron–hole pairs become localized and subsequently radiatively recombine. In order to continue this dependence to the region of smaller standard deviations for the x and y coordinates, a large number of photocounts is required. For example, to attain an accuracy on the order of 1 nm, it is necessary to accumulate 50,000 photocounts, which encounters a number of obstacles related to the photostability of the investigated emitters and the effective dynamic range of electron multiplying CCD cameras.

To overcome these difficulties, we carried out measurements with a small exposure, equal to 100 ms (which yielded at most 1000 photons per image). The obtained images of single quantum dots were processed and sorted according to the fluorescence intensity. Afterwards, the images were grouped on the basis of the chosen intensity level and further processed statistically, which made it possible to obtain an effective intensity corresponding to the required accuracy of coordinate reconstruction. In this way, we were able to attain an accuracy of coordinate reconstruction better than 0.5 nm, which is about 10% the core size of a single quantum dot.

In order to check that the coordinate reconstruction accuracy attained in this way is physically meaningful, we performed the following sophisticated experiment. A sample with single quantum dots embedded in a thin polymer film on a glass substrate was placed on a piezo-driven microscope stage (NanoScanTech). The stage positioning accuracy was just a few angstroms, which was ensured by feedback using calibrated capacitive sensors. The sample was shifted with a step of 2 nm along one axis, after which the quantum dot images were repetitively measured and analyzed. As a result, a set of single quantum dot coordinates corresponding to different spatial positions of the sample was obtained.

Figure 7c shows the dependence of the reconstructed coordinates of a single quantum dot on the actual spatial shift of the sample. The indicated error bars correspond to the accuracies of coordinate reconstruction and stage positioning (< 5 Å). One can see that, in this example, there is good agreement (within the indicated error) between the actual and measured shifts of the emissive center of the quantum dot. This means that the standard deviation obtained in this way determines the accuracy with which shifts of an SQE emitting center can be monitored.

These results are interesting in view of the studies of interaction processes in systems like several closely spaced quantum dots. One such system is a cluster of giant quantum dots with fused shells [62], where the observed antibunching was attributed to the processes of Auger ionization involving excitons localized in different cores of the cluster. Other examples include quantum dot chains [63] and pairs [64]. The high accuracy of spatial localization of the emissive center opens the way to the investigation of interaction processes in such systems at the level of individual quantum emitters.

5. Conclusions

The entire system of experimental techniques, instruments, and software algorithms combined in the multifunctional far-field luminescence nanoscope described in this paper provides unique capabilities for the investigation of photophysical properties of SQEs of various nature and chemical compositions, as well as composite materials and structures based on them. The developed hardware/software facility makes it possible to study intra- and intermolecular processes at the level of individual molecules and molecular complexes and single quantum dots. For example, the microscopic origin of the effect of luminescence intermittence in colloidal semiconductor nanocrystals (quantum dots) was clarified in the studies presented here.

The serial–parallel detection of the spectra and fluorescence images of a large number of dopant SQEs used as markers with the subsequent processing of large databases offers the possibility of multiparameter nanodiagnostics of materials. In particular, we have developed approaches to the subwavelength mapping of material parameters of solid films. We have attained record accuracy in reconstructing the coordinates of single molecules and colloidal semiconductor quantum dots.

The developed methods and approaches may find applications in a broad range of fundamental and applied problems of modern materials science, nanotechnologies, quantum technologies, and microelectronics.

Acknowledgments
Part of this work on 'Statistical methods of investigation of luminescence from single nanoobjects' was supported by the Russian Science Foundation (project no. 14-02-01415). Work on the development of the techniques for superresolution

microscopy with semiconductor quantum dots (I E, M E) was supported by a grant from the President of the Russian Federation for young PhDs (project no. MK-2184.2017.2). Some of the studies reviewed here were supported by the Presidium of the Russian Academy of Sciences under its Program I.7, "Current Problems in Photonics, Probing of Inhomogeneous Media and Materials" and the State Assignment for the Institute of Spectroscopy, Russian Academy of Sciences.

References

1. Moerner W E *Angew. Chem. Int. Ed.* **54** 8067 (2015)
2. Betzig E *Angew. Chem. Int. Ed.* **54** 8034 (2015)
3. Hell S W *Angew. Chem. Int. Ed.* **54** 8054 (2015)
4. Henriques R et al. *Nature Meth.* **7** 339 (2010)
5. Jones S A et al. *Nature Meth.* **8** 499 (2011)
6. von Diezmann A, Shechtman Y, Moerner W E *Chem. Rev.* **117** 7244 (2017)
7. Bates M et al. *Science* **317** 1749 (2007)
8. Naumov A V *Phys. Usp.* **56** 605 (2013); *Usp. Fiz. Nauk* **183** 633 (2013)
9. Hofmann C et al. *Phys. Rev. Lett.* **90** 013004 (2003)
10. Nirmal M et al. *Nature* **383** 802 (1996)
11. Dvurechenskii A V, Yakimov A I *Phys. Usp.* **44** 1304 (2001); *Usp. Fiz. Nauk* **171** 1371 (2001)
12. Razumov V F *Phys. Usp.* **59** 1258 (2016); *Usp. Fiz. Nauk* **186** 1368 (2016)
13. Osad'ko I S *Phys. Usp.* **59** 462 (2016); *Usp. Fiz. Nauk* **186** 489 (2016)
14. Doherty M W et al. *Phys. Rep.* **528** 1 (2013)
15. Mishin A S et al. *Curr. Opin. Chem. Biol.* **27** 1 (2015)
16. Turchin I V *Phys. Usp.* **59** 487 (2016); *Usp. Fiz. Nauk* **186** 550 (2016)
17. Doronina-Amitonova L V et al. *Phys. Usp.* **58** 345 (2015); *Usp. Fiz. Nauk* **185** 371 (2015)
18. Kinkhabwala A et al. *Nature Photon.* **3** 654 (2009)
19. Vinogradov A P et al. *Phys. Usp.* **55** 1046 (2012); *Usp. Fiz. Nauk* **182** 1122 (2012)
20. Krasnok A E et al. *Phys. Usp.* **56** 539 (2013); *Usp. Fiz. Nauk* **183** 561 (2013)
21. Vitukhnovsky A G *Phys. Usp.* **54** 1268 (2011); *Usp. Fiz. Nauk* **181** 1341 (2011)
22. Vitukhnovsky A G *Phys. Usp.* **56** 623 (2013); *Usp. Fiz. Nauk* **183** 653 (2013)
23. Vinogradov A P, Dorofeenko A V, Zouhdi S *Phys. Usp.* **51** 485 (2008); *Usp. Fiz. Nauk* **178** 511 (2008)
24. Brinks D et al. *Chem. Soc. Rev.* **43** 2476 (2014)
25. Naumov A V et al. *Phys. Rev. B* **63** 212302 (2001)
26. Vainer Yu G, Naumov A V, Bauer M, Kador L *Phys. Rev. Lett.* **97** 185501 (2006)
27. Eremchev I Yu, Naumov A V, Vainer Yu G, Kador L *J. Chem. Phys.* **130** 184507 (2009)
28. Naumov A V et al. *Angew. Chem. Int. Ed.* **48** 9747 (2009)
29. Naumov A V et al. *Phys. Chem. Chem. Phys.* **13** 1734 (2011)
30. Eremchev I Y, Vainer Y G, Naumov A V, Kador L *Phys. Chem. Chem. Phys.* **13** 1843 (2011)
31. Osad'ko I S et al. *Phys. Rev. A* **86** 053802 (2012)
32. Eremchev I Y, Vainer Y G, Naumov A V, Kador L *Phys. Solid State* **55** 710 (2013); *Fiz. Tverd. Tela* **55** 652 (2013)
33. Anikushina T A, Gladush M G, Gorshelev A A, Naumov A V *Faraday Discuss.* **184** 263 (2015)
34. Osad'ko I S, Eremchev I Yu, Naumov A V *J. Phys. Chem. C* **119** 22646 (2015)
35. Eremchev I Yu, Osad'ko I S, Naumov A V *J. Phys. Chem. C* **120** 22004 (2016)
36. Naumov A V et al. *Nano Lett.* **18** 6129 (2018)
37. Naumov A, Eremchev I Yu, Gorshelev A A *Eur. Phys. J. D* **68** 348 (2014)
38. Moerner W E, Kador L *Phys. Rev. Lett.* **62** 2535 (1989)
39. Orrit M, Bernard J *Phys. Rev. Lett.* **65** 2716 (1990)
40. Güttler F et al. *Chem. Phys. Lett.* **217** 393 (1994)
41. van Oijen A M et al. *Chem. Phys. Lett.* **292** 183 (1998)
42. Weiss S *Science* **283** 1676 (1999)
43. Eid J et al. *Science* **323** 133 (2009)
44. Dittrich P S, Manz A *Nature Rev. Drug Discov.* **5** 210 (2006)
45. Mehta S B et al. *Proc. Natl. Acad. Sci. USA* **113** E6352 (2016)
46. Rust M J, Bates M, Zhuang X *Nature Meth.* **3** 793 (2006)
47. Betzig E et al. *Science* **313** 1642 (2006)
48. Efros A L, Nesbitt D J *Nature Nanotechnol.* **11** 661 (2016)
49. Shirasaki Y et al. *Nature Photon.* **7** 13 (2013)
50. Jelezko F, Wrachtrup J *Phys. Status Solidi A* **203** 3207 (2006)
51. Chizhik A I et al. *Nano Lett.* **11** 1700 (2011)
52. Türschmann P et al. *Nano Lett.* **17** 4941 (2017)
53. Mochalov K E et al. *ACS Nano* **7** 8953 (2013)
54. Fischer T et al. *Nano Lett.* **17** 1559 (2017)
55. Wolff G et al. *Biol. Cell* **108** 245 (2016)
56. Wei Q et al. *ACS Nano* **8** 12725 (2014)
57. Pavani S R P et al. *Proc. Natl. Acad. Sci. USA* **106** 2995 (2009)
58. Volostnikov V G *Phys. Usp.* **55** 412 (2012); *Usp. Fiz. Nauk* **182** 442 (2012)
59. Volostnikov V G et al. *Bull. Russ. Acad. Sci. Phys.* **80** 766 (2016); *Izv. Ross. Akad. Nauk Ser. Fiz.* **80** 841 (2016)
60. Savostianov A O et al. *JETP Lett.* **107** 406 (2018); *Pis'ma Zh. Eksp. Teor. Fiz.* **107** 426 (2018)
61. Mortensen K I et al. *Nature Meth.* **7** 377 (2010)
62. Lv B et al. *Nature Commun.* **9** 1536 (2018)
63. Koole R et al. *J. Am. Chem. Soc.* **128** 10436 (2006)
64. Eremchev I Yu et al. *JETP Lett.* **108** 30 (2018); *Pis'ma Zh. Eksp. Teor. Fiz.* **108** 26 (2018)